xNi–yCu–ZrO₂ catalysts for the hydrogenation of levulinic acid to gamma valorlactone

Daniel R. Jones, Sarwat Iqbal, Liam Thomas, Satoshi Ishikawa, Christian Reece, Peter J. Miedziak, David J. Morgan, Jonathan K. Bartley, David J. Willock, Wataru Ueda & Graham J. Hutchings

Taylor & Francis
Taylor & Francis Group

OPEN ACCESS

Check for updates

xNi–yCu–ZrO$_2$ catalysts for the hydrogenation of levulinic acid to gamma valorlactone

Daniel R. Jones[a], Sarwat Iqbal[a] (ID), Liam Thomas[a], Satoshi Ishikawa[a,b] (ID), Christian Reece[a], Peter J. Miedziak[a], David J. Morgan[a], Jonathan K. Bartley[a], David J. Willock[a] (ID), Wataru Ueda[b,c] and Graham J. Hutchings[a]

[a]Cardiff Catalysis Institute, Cardiff, UK.; [b]Catalysis Research Center, Hokkaido University, Sapporo, Japan; [c]Department of Material and Life Chemistry, Faculty of Engineering, Kanagawa University, Kanagawa-ku, Yokohama, Japan

ABSTRACT

We have investigated xNi–yCu–ZrO$_2$ catalysts for the selective synthesis of γ-valerolactone from levulinic acid (LA). A series of xNi–yCu–ZrO$_2$ catalysts with a consistent metal loading of 50% but varying Ni and Cu composition were prepared by an oxalate gel precipitation method and tested for LA hydrogenation. Ni-rich catalysts showed higher catalytic activity compared with Cu-rich formulations with a 45Ni–5Cu–ZrO$_2$ composition yielding 76% γ-valerolactone after a reaction time of 30 min at 200 °C. Characterisation of the materials by XRD, surface area measurements and TPR allow us to attribute the differences in performance seen for different compositions to particle size and nanoparticle dispersion effects. DFT calculations also showed that a shift of d-band centre to higher energies with the mole fraction of Ni in Cu–Ni alloys would be expected to lead to improved hydrogen dissociation in Ni-rich catalysts and so aid hydrogenation activity.
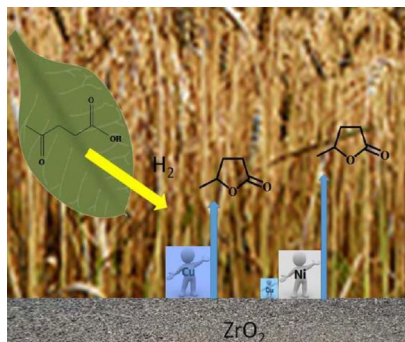
Introduction

Utilisation of biomass for the production of fuel and chemicals has become an important research topic because of growing concerns about the finite nature of fossil carbon reserves and the environmental impact of our continued dependence on these resources. Recently, levulinic acid (LA) was included in a list of the "Top 10" building blocks for future biorefineries as proposed by the US department of energy [1]. LA is considered one of the most important platform molecules for the production of fine chemicals and fuels [2] based on its compatibility with existing processes, market economics, industrial viability and ability to serve as a platform for the synthesis of important derivatives. Hydrogenation of LA to produce γ-valerolactone (GVL) is an active area of research due to the potential

of GVL to be used as a biofuel in its own right and for its subsequent transformation into hydrocarbon fuels [3]. The hydrogenation of LA to GVL has been reported using both homogeneous and heterogeneous catalysts [4,5]. Re, Ru, Pd, and Pt have been the generally explored precious metal heterogeneous catalysts for the synthesis of GVL from LA with a particular focus on Ru due to its excellent performance for the liquid phase hydrogenation of this substrate [6–9]. High turnover numbers can also be achieved using well dispersed Pd nanoparticles deposited on SiO$_2$ supports [10]. Ir on polymer supports [11], Sn/SBA-15 [12] and Pt–Pd/SBA-15 [13] have also been identified as active catalysts for this hydrogenation reaction.

However, for a process to become truly sustainable, not only do the substrates need to be renewable but

also the catalysts used for their transformation should be inexpensive and abundant in nature. Cu is one of the most abundant and relatively cheap metals that has been reported to be active for LA hydrogenation making it a desirable replacement for precious metal based catalysts [5,14,15]. We have recently shown that the oxalate gel co-precipitation method coupled with a pre-reduction of the catalyst prior to use can significantly enhance the activity of Cu–ZrO$_2$ catalysts compared to alternative preparation methods. Zirconia is a particularly well suited material for this catalyst system as Cu can be incorporated into the ZrO$_2$ lattice through co-precipitation. This provides effective anchor points for the Cu nanoparticles which prove to be the active component of the resulting hydrogenation catalyst [5,16]. Our conclusions on the role of each component of these materials in the structure of the catalysts are in line with earlier work using similar catalysts for the steam reforming of methanol [17]. However, the scope of application in the area of hydrogenation chemistry for aqueous phase substrates such as LA has been less well investigated. In general hydrogenation catalysis studies have either relied on the traditional precious metals or applied the same impregnation/deposition methods used to form metal nanoparticles for those catalysts to the synthesis of materials with copper as the active component. For example, Cu–Ni/Al$_2$O$_3$, with Ni the minor component, prepared by incipient impregnation has been reported [18] and showed 50% GVL yield after 2 h of reaction at 150 °C for the catalytic transfer hydrogenation of ethyl levulinate.

Whilst we have shown how Cu–ZrO$_2$ catalysts produced via the oxalate gel route can give high activity and selectivity for the hydrogenation of LA to GVL, the reaction conditions required are more forcing than used with supported Ru or Pd catalysts. In this work, we have considered the possibility of alloying Cu with Ni to enhance the catalytic performance further. Once again, the catalyst preparation is key and we consider the effects of alloy composition and post-synthesis reduction temperature on catalyst performance. These are shown to have a significant effect on catalyst performance with some alloy compositions giving higher activity that either single metal. The source of the synergy is discussed in the light of extensive materials characterisation and DFT calculations.

Ni has been selected as a second low cost and abundant metal component for these catalysts. Supported nickel alone has already shown catalytic potential for various hydrogenation processes. Ni supported on γ-Al$_2$O$_3$ has been used by Hengst et al. to produce GVL with 100% selectivity with water as solvent [19]. The same work also showed high yields of GVL under solvent free conditions. Rao and co-workers reported 30 wt.% Ni/SiO$_2$ prepared by a wet impregnation method; as an active catalyst which showed full conversion of LA with 85–90% selectivity to GVL [20]. Further they compared

SiO$_2$ with other oxide supports including Al$_2$O$_3$, ZrO$_2$, TiO$_2$, ZnO, and MgO. Ni/Al$_2$O$_3$ showed comparable conversions of LA, whereas Ni/TiO$_2$, Ni/ZnO, and Ni/MgO performed poorly due to lower Ni dispersion on the surface and low support acidity. The catalyst synthesised as Ni supported on zirconia, Ni/ZrO$_2$, also performed poorly because catalytic activity was hindered by large Ni particle sizes and low Ni dispersion.

Mohan et al. demonstrated that a 30 wt.% Ni/H-ZSM-5 catalyst was able to produce high yields of GVL (90%) and that the Ni dispersion is an important feature for catalytic activity [21]. Stability was also an issue in this case, with GVL yield decreasing to 65% after just 5 h, possibly as a result of water generated during the reaction. Varkolu et al. reported Ni supported on Al$_2$O$_3$, MgO, and hydrotalcite which also exhibited the same deactivation because of water generated during the reaction [22]. MgO and hydrotalcite supports showed a drastic decline in activity due to phase changes caused by interaction with water. Al$_2$O$_3$ was also affected by water, though to a lesser extent. Shimizu et al. showed that Ni can be modified with MoO$_x$ to give an improvement in hydrogenation activity [23]. They report that the turn over number of the Ni–MoO$_x$/C catalyst is comparable to the performance of the commonly used Ru based catalyst, however a high temperature of 250 °C is required and catalyst stability is not considered.

Catalysts containing a mix of Cu and Ni have also been reported to improve activity for hydrogenation reactions. Upare et al. [24] have reported that Ni added to a Cu/SiO$_2$ system can alleviate the stability problems suffered by Cu/SiO$_2$ alone. They report a 96% yield of GVL at 265 °C and 25 bar of H$_2$. This catalyst was also used by the same research group to hydrogenate LA using formic acid as a H$_2$ source, and was stable up to 100 h on stream [25]. Arias and co-workers investigated the effect of Ni–Cu catalysts supported on Al$_2$O$_3$ for LA hydrogenation to 2-MTHF, which occurs via GVL as an intermediate [26]. Ni/Al$_2$O$_3$ was found to be the most active catalyst, and Cu/Al$_2$O$_3$ the most selective to 2-MTHF. An optimum combination of the two metals resulted in a yield of 56% 2-MTHF in 5 h at 250 °C which is the highest yield achieved by a non-noble metal catalyst so far. The authors concluded that there was a synergistic effect between Ni and Cu in the mixed Ni–Cu particles leading to an improved yield of 2-MTHF. A recent study by Palkovits and co-workers [27] discussed the mechanism of the hydrogenation of LA to GVL and 2-MTHF using Cu–Ni/Al$_2$O$_3$ catalyst under hydrogenation and transfer hydrogenation conditions. They have reported that Cu–Ni/Al$_2$O$_3$ catalysts are more active than Ru/C using a solvent that is a poor hydrogen donor, and that a 93% yield of GVL can be obtained.

The above literature shows that attempts have been made to show positive effects of bimetallic (Cu–Ni) catalysts for LA hydrogenation using supported metal catalysts. Co-precipitation of metal and oxide support is less

widely employed but offers a route to high levels of metal dispersion. We have recently shown the effect of catalyst preparation parameters on Cu–ZrO$_2$ for GVL synthesis from LA [5]. Now, we have investigated the effect of Ni addition into the Cu–ZrO$_2$ catalyst and have identified a profound effect on catalytic activity when bimetallic Cu–Ni catalysts are used. To our knowledge, this is the first study to report the effect of alloy composition and preparation variables on the performance of xNi–yCu–ZrO$_2$ catalysts prepared by the oxalate gel method for the LA hydrogenation reaction.

Experimental

Catalyst preparation

Oxalate gel method

The catalysts were prepared by the oxalate gel (OG) method. In a typical synthesis Cu(NO$_3$)$_2$ 3H$_2$O (0.01 mol, Sigma Aldrich), Ni(NO$_3$)$_2$ 6H$_2$O (0.01 mol, Sigma Aldrich) and ZrO(NO$_3$)$_2$ 6H$_2$O (0.01 mol, Archos Organics, UK) were dissolved in ethanol (200 mL). The composition of the material was determined by the molar ratio of the metal content of the catalyst. So that a material referred to as xNi–yCu–ZrO$_2$ contains x molar % Ni and y molar % Cu referred to the total moles of Ni, Cu and Zr present. All materials compared in this work have $x + y = 50$ mol%. Oxalic acid (0.024 mol, Sigma Aldrich) was added and the resulting precipitates were aged in the mother liquor at room temperature for 2 h. The precipitate was then filtered without a washing step. The material was dried (110 °C, 16 h), calcined (550 °C (heating rate 10 °C min^{-1}) in static air, 2 h), followed by reduction at the desired temperature in a flow of 5% H$_2$/Ar (heating rate 10 °C min^{-1}) for 2 h.

Characterization

Powder X-ray diffraction (PXRD) was performed using a PANalytical X'Pert Pro fitted with an X'Celerator detector and a Cu Kα X-ray source operated at 40 kV and 40 mA, 2θ = 10–80°. Each sample was scanned from 2θ = 10° to 80° for 30 min. The catalysts were ground into fine powder before the analysis. The results obtained were compared with the information in SPDF library for each catalyst.

Microwave plasma atomic emission spectroscopy (MP-AES) was performed using an Agilent 4100 MP-AES machine. The samples were introduced to the nitrogen plasma using a single pass spray chamber at a pressure of 120 kPa without air injection. The instrument was calibrated with 1, 2, 4, 7, 10 ppm standard solutions in 10% HCl. The samples were tested in triplicate and the average result was used. Cu content was analysed with two emission lines at 324.754 and 327.395 nm and Ni content was analysed with two lines at 341.476 and 352.454 nm.

Temperature programmed reduction (TPR) was carried out using a Thermo 1100 series TPDRO under 75 ml min^{-1} 5% H$_2$/Ar, 10 °C min^{-1} ramp rate. Samples (0.1 g) sandwiched between quartz wool were pre-treated at 110 °C (heating rate = 20 °C min^{-1}) under Ar for 1 h prior to reduction in order to clean the surface. After cooling to ambient temperature, analysis was performed under 10% H$_2$/Ar (25 ml min^{-1}) between 30 and 800 °C (heating rate 10 °C min^{-1}).

X-ray photoelectron spectroscopy (XPS) was performed using a Kratos Axis Ultra-DLD photoelectron spectrometer, using monochromatic Al kα radiation, operating at 144 W power. High resolution and survey scans were performed at pass energies of 40 and 160 eV respectively. Spectra were calibrated to the C (1s) signal at 284.8 eV and quantified using Casa XPS v2.3.17, using modified Wagner sensitivity factors supplied by the manufacturer.

Brunauer–Emmett–Teller (BET) surface areas were determined by multi-point N$_2$ adsorption at 77 K on a Micromeretics Gemini 2360. Prior to the analysis, samples were degassed at 120 °C for 1 h under N$_2$ flow.

N$_2$O titration was performed on a Quantachrome ChemBet equipped with a zeolite trap for the prepared catalysts. Prior to the analysis, the catalysts were reduced $in\ situ$ under 30 ml min^{-1} of 10% H$_2$/Ar flow at 180 °C. Then the temperature was decreased to 65 °C with He purging in order to remove H$_2$ adsorbed on the catalyst surface. N$_2$O was pulsed until no signals due to N$_2$ formation were detected using a TCD detector. After titration, a known amount of N$_2$ was fed for calibration.

LA hydrogenation

Reactions were carried out using a 50 mL, Parr Instruments, Model 5500HP stainless steel stirred autoclave equipped with a Teflon liner. Typically, the liner was charged with the desired amounts of catalyst and substrate (LA) and sealed inside the autoclave. The sealed autoclave was purged three times with N$_2$ in order to remove residual air, and three times with H$_2$ to remove residual N$_2$ before being pressurised to the required reaction pressure with H$_2$. The autoclave was heated to the required temperature. The stirring rate was increased to 2000 rpm when the reaction temperature was reached, which was considered to be the start of the reaction ($t = 0$). When the reaction was completed, the autoclave was rapidly cooled in an ice bath in order to quench the reaction. The gasses were vented when the temperature was <10 °C and a sample of the vented gases captured and analysed using GC. For all reactions the gas phase products were detected at only very low levels (<0.1% by mass of converted substrate). The catalyst was filtered using filter paper and the reaction solution was analysed using an offline Varian 450 GC equipped with CP-Sil 5CB (50 m, 0.32 mm, 5 μm) column and detected

by an FID detector. Helium was used as the carrier gas. For the analysis acetonitrile (0.1 mL) was added to the reaction solution (0.9 mL) as an external standard. The GC was calibrated to obtain response factors both for reactant and the possible products. Carbon mass balance was calculated for every reaction individually and was always above 95%. Therefore, the reaction data are presented in terms of product yield.

Catalyst reuse studies

In order to carry out the catalyst reuse studies an excess of catalyst was used for LA hydrogenation. After the completion of reaction with a large batch of catalyst (approx. 0.5 g), we took out the amount of catalyst used under our standard conditions (0.05 g) for the reaction and obtained the data for LA conversion (GVL yield). This is the data we reported not the one from large batch. Then we used the rest of the catalyst (0.5–0.05 g) and after filtration, drying steps we again used a standard conditions aliquot of catalyst (0.05 g) from this second reuse for the reaction and obtained data for LA conversion (GVL analysis).

Computational methods

Spin unrestricted periodic DFT calculations were performed using projector augmented wave method (PAW) [28,29] pseudopotentials within the VASP program [30–33]. Calculations were performed within a generalized gradient approximation using the exchange-correlation functional of Perdew, Burke and Ernzerhof (PBE) [34,35]. All density of states (DOS) calculations were performed using a k-point sampling mesh of $11 \times 11 \times 11$ along with a 500 eV cut-off for plane wave interactions. Structures of bulk Ru, Ni and Cu were prepared through a ±5% expansion of the unit cells in steps of 0.5% to locate energy minima by fitting of a quadratic function to the 5 points closest to the predicted minima.
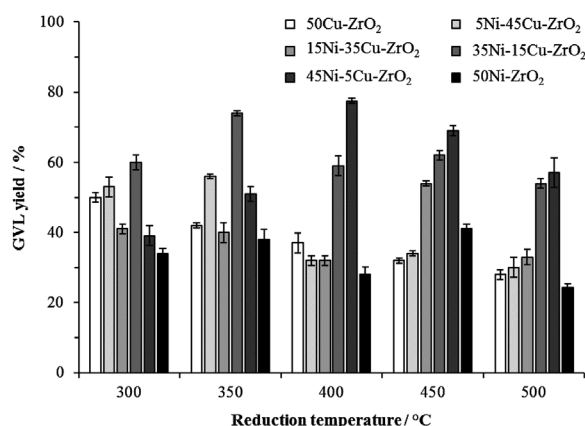

Figure 1. Catalytic activity of xNi–yCu–ZrO$_2$ catalysts prepared with different compositions and reduction temperatures. *Reaction conditions*: 200 °C, 35 bar H$_2$, 30 min, 5 wt.% LA/H$_2$O, catalyst (0.05 g).

The lattice parameters obtained by this method where closely comparable to the experimental literature (Ru: $a = b = 2.7059$ Å, $c = 4.2815$ Å, Ni: $a = b = c = 3.524$ Å, Cu: $a = b = c = 3.6149$ Å).

Results and discussion

50Cu–ZrO$_2$, xNi–yCu–ZrO$_2$ of various compositions with $x + y = 50$, and 50Ni–ZrO$_2$ catalysts were prepared by the OG method. In our earlier work with Cu–ZrO$_2$ catalysts it was shown that hydrogenation activity can be greatly improved by reducing the catalyst with H$_2$ prior to use [16]. Accordingly, these catalysts were reduced at different temperatures using 5% H$_2$/Ar (after calcination at 550 °C). Each catalyst was then investigated for its activity for the conversion of LA into GVL, and the results are presented in Figure 1. Analysis of the GC data showed GVL and unconverted LA only, confirming that each catalyst gives 100% selectivity to GVL under the reaction conditions used and no by-products are formed. For the catalysts containing only Cu, the 50Cu–ZrO$_2$ catalyst reduced at 300 °C was the most active and produced a GVL yield of 50% after 30 min. Increasing the temperature of the pre-reduction step for this material lead to lower yields of GVL with 50Cu–ZrO$_2$ reduced at 500 °C producing a GVL yield of only 28% under the same experimental conditions. Catalysts prepared with only Ni, 50Ni–ZrO$_2$, gave consistently low GVL yields, regardless of the reduction temperature, with a maximum GVL yield of 40% produced after 30 min for the materials pre-reduced at 450 °C. For xNi–yCu–ZrO$_2$ catalysts, Ni-rich materials were generally more active than the Cu-rich catalysts. Amongst the set of mixed metal xNi–yCu–ZrO$_2$ catalysts the 35Ni–15Cu–ZrO$_2$ catalyst pre-reduced at 350 °C and 45Ni–5Cu–ZrO$_2$ pre-reduced at 400 °C showed a comparable yield of GVL (72% and 76% respectively) after 30 min of reaction. The single metal catalyst 50Ni–ZrO$_2$ showed relatively poor activity for all reduction temperatures. So it appears that small amounts of Cu in xNi–yCu–ZrO$_2$ materials results in the most active catalysts.

The Ni–ZrO$_2$, and xNi–yCu–ZrO$_2$ catalysts prepared and reduced at 400 °C were investigated further because the most active catalyst (45Ni–5Cu–ZrO$_2$) was contained within this group, and the group showed a clear difference in activity between the catalysts with a high Ni content (35Ni–15Cu–ZrO$_2$ and 45Ni–5Cu–ZrO$_2$) and low Ni contents (5Ni–45Cu–ZrO$_2$ and 15Ni–35Cu–ZrO$_2$). The data from this group was also compared with 50Cu–ZrO$_2$ reduced at 300 °C as this materials showed the highest activity of the Cu only catalysts. The reaction profiles of each of these catalysts for reaction times between 0 and 90 min are shown in Figure 2. 50Cu–ZrO$_2$, 35Ni–15Cu–ZrO$_2$, and 45Ni–5Cu–ZrO$_2$ achieved 100% GVL yield after 90, 75, and 55 min respectively. The other catalysts: 50-Ni–ZrO$_2$, 15Ni–35Cu–ZrO$_2$, and 5Ni–45Cu–ZrO$_2$ –show a lower initial rate up to 30 min
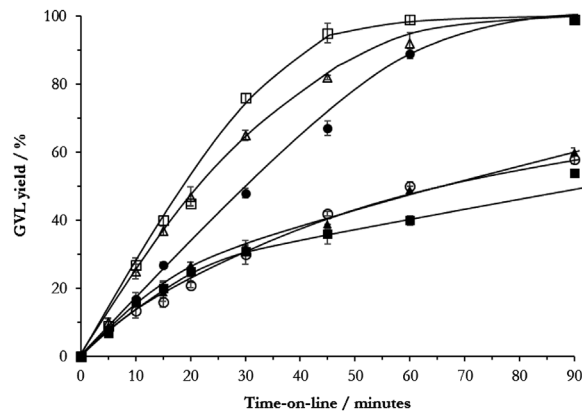
Figure 2. Time-on-line data for xNi–yCu–ZrO$_2$ prepared with different Ni–Cu compositions reduced at 400 °C. *Reaction conditions*: 200 °C, 35 bar H$_2$, 5 wt.% LA/H$_2$O, catalyst (0.05 g) ●: 50Cu–ZrO$_2$ (pre-reduced at 300 °C); ■: 5Ni–45Cu–ZrO$_2$; ▲: 15Ni–35Cu–ZrO$_2$; Δ: 35Ni–15Cu–ZrO$_2$; □: 45Ni–5Cu–ZrO$_2$; ○: 50Ni–ZrO$_2$.

Table 1. Initial rates and TONs for Cu–ZrO$_2$, Ni–ZrO$_2$, and xNi–yCu–ZrO$_2$ catalysts.

Catalyst	Initial rate of reaction/ mol dm^{-3} s^{-1}	TON at 30 min/g$_{GVL}$ g$_{cat}^{-1}$
50Cu–ZrO$_2$	8.26×10^{-5}	1.71×10^{-3}
5Ni–45Cu–ZrO$_2$	6.43×10^{-5}	1.14×10^{-3}
15Ni–35Cu–ZrO$_2$	6.43×10^{-5}	1.14×10^{-3}
35Ni–15Cu–ZrO$_2$	1.21×10^{-4}	2.31×10^{-3}
45Ni–5Cu–ZrO$_2$	1.32×10^{-4}	2.70×10^{-3}
50Ni–ZrO$_2$	5.56×10^{-5}	1.06×10^{-3}

Notes: *Reaction conditions*: 200 °C, 35 bar H$_2$, 30 min, 5 wt.% LA/H$_2$O, catalyst (0.05 g). Linear fits for initial rates are shown in figure S1. All samples pre-reduced at 400 °C, except 50Cu–ZrO$_2$ (pre-reduced at 300 °C).

and did not proceed to completion within a reaction time of 90 min.

Because the reaction profiles were linear for the initial 30 min, the initial rates and turnover numbers (TON) were calculated for each of these catalysts to give the results shown in Table 1. These values are comparable to the values reported previously with 50Cu–ZrO$_2$ catalysts (initial rate: 8.2×10^{-5} mol dm^{-3} s^{-1}) [16]. From these data the Ni rich catalyst, 45Ni–5Cu–ZrO$_2$ shows the highest initial rate and TON factors around 60% greater than that for the monometallic 50Cu–ZrO$_2$ catalyst and more than twice that of 50Ni–ZrO$_2$.

Additional kinetic measurements were carried out using the most active catalyst – 45Ni–5Cu–ZrO$_2$ reduced at 400 °C. For this purpose the yield of GVL was calculated from GC measurements and the rate of reaction was determined from the gradient of GVL concentration (mol dm^{-3}) vs. time (s). Figure 3 shows the dependence of GVL concentration after 30 min reaction on the effective concentration of reactants. From these plots the order of reaction for GVL production from LA for the LA and H$_2$ reagents can be obtained. The reaction was found to be zero order in LA. This agrees with previous reports of zero order behaviour for the hydrogenation of LA using Cu–ZrO$_2$ [16] and Ru [36] catalysts and suggests that LA is in

excess at the catalyst surface. At low H$_2$ pressure, the reaction is first order with respect to H$_2$, but tends to a zero order dependence for H$_2$ at pressures above 40 bar. Accordingly, at low H$_2$ pressure, the rate determining step is likely to be the dissociation of H$_2$ as reported previously [36]. At higher pressures the surface becomes saturated with H$_2$ and the rate is no longer affected by increasing the H$_2$ pressure. This behaviour with respect to H$_2$ concentration has also been observed in studies utilising high H$_2$ pressures and Ru catalysts for LA hydrogenation [37,38].

XRD patterns were obtained for all of the catalysts prepared at various Cu:Ni ratios and using a reduction temperature of 400 °C, these are compared to the most active Cu only material (reduced at 300 °C) in Figure 4. The most prominent reflections can be assigned to t-ZrO$_2$ (ICDD: 01-080-2155) at $2\theta = 30.6°$, 51.4°, 61.0° and 74.5°, and these are observed in all catalysts although with varying intensity. Reflections at $2\theta = 35°$, 37° and 63° corresponding to NiO (ICDD: 01-089-7101) can be seen for the catalysts with higher amounts of Ni (35Ni–15Cu–ZrO$_2$, 45Ni–5Cu–ZrO$_2$ and 50Ni–ZrO$_2$). In 50Ni–ZrO$_2$ there were two reflections at $2\theta = 43.6°$ and 44.2° the former corresponding to NiO and the latter corresponding to Ni metal (ICDD: 03-065-0360). Figure 4(b) shows a 4° section of the diffraction patterns shown in Figure 4(a) to highlight an interesting change in the XRD patterns between $2\theta = 43°–46°$ in the bimetallic catalysts. A reflection corresponding to Cu metal was observed at 43.3° in the 50Cu–ZrO$_2$ catalyst but this is shifted to a higher diffraction angles for the xNi–yCu–ZrO$_2$ materials. This shift gradually increased from 43.5° to 44.2° from 5Ni–45Cu–ZrO$_2$ to 45Ni–5Cu–ZrO$_2$ respectively. There were no other peak shifts observed in the bimetallic catalyst relating to any other phases. This shift implies that an alloy of Cu and Ni (ICDD: 01-071-7847) has formed in all bimetallic catalysts [39,40], with the presence of Ni shifting the reflection in all bimetallic catalysts to values between $2\theta = 43.3°$ (Cu metal: 50Cu–ZrO$_2$) to $2\theta = 44.2°$ (Ni metal: 50Ni–ZrO$_2$). With an increase in Ni-content, the intensity of the alloy reflection decreases to the point where it can hardly be observed in the XRD pattern of 45Ni–5Cu–ZrO$_2$.

The Scherrer equation was used to calculate the particle size from the diffraction peaks in the 42–46° range (Table 2). The data shows that there was a decrease in alloy particle size with an increase in Ni-content. 35Ni–15Cu–ZrO$_2$ and 45Ni–5Cu–ZrO$_2$ were the more active xNi–yCu–ZrO$_2$ catalysts and both had small alloy particle sizes as implied by the XRD data. This suggests that a small particle size leads to a high catalytic activity, and that the synthesis of small metal particle sizes can be achieved by increasing the Ni-content in the mixed metal catalysts.

BET and N$_2$O titration for the determination of total surface area and metal surface area respectively were carried out for each of the materials reduced at 400 °C
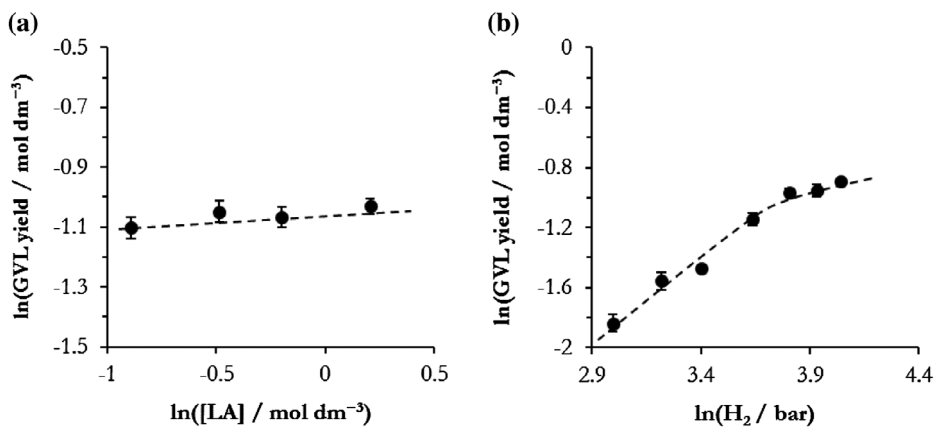
Figure 3. Dependency of GVL yield on reagent concentrations for determining reaction order for (a) LA, and (b) H$_2$. *Reaction conditions*: in both cases 200 °C, 30 min reaction, 45Ni–5Cu–ZrO$_2$ reduced at 400 °C (0.05 g). For (a) 35 bar H$_2$, and for (b) 5 wt.% LA/H$_2$O.
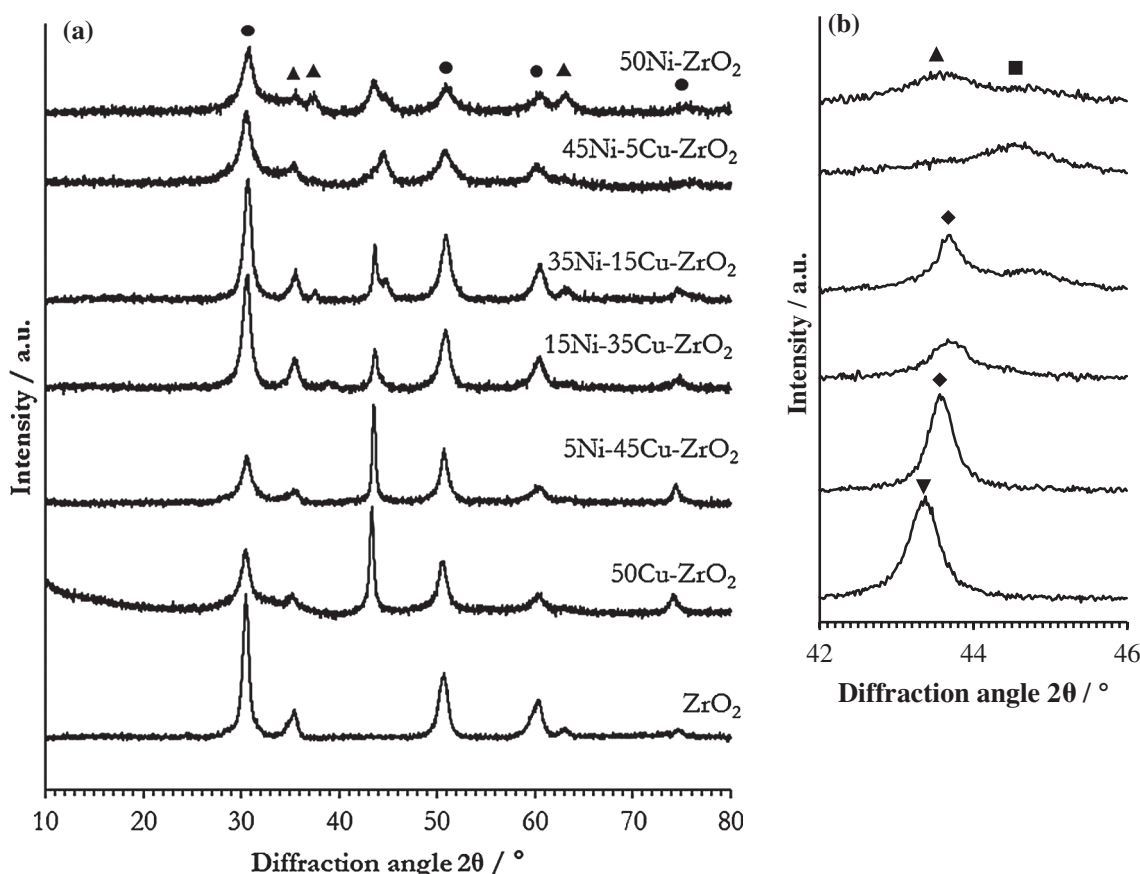

Figure 4. XRD patterns of *x*Ni–*y*Cu–ZrO$_2$ catalysts, reduced at 400 °C and 50Cu–ZrO$_2$ reduced at 300 °C. (a): Full diffraction pattern; (b): diffraction pattern zoomed to show 2θ = 42–46° traces are aligned with the material of the same composition in (a). Reflections due to known phases are marked as: ●: ZrO$_2$; ▲: NiO; ■: Ni; ▼: Cu; ◆: Cu–Ni.

(except for 50Cu–ZrO$_2$, which was reduced at 300 °C). Since both Cu and Ni can undergo oxidation by N$_2$O, the surface area cannot be assigned to a specific element, therefore total N$_2$O adsorption is reported (Table 2). These data show that both the BET surface area and specific adsorption of N$_2$O were affected by varying the Cu–Ni composition of the catalyst. The 50Cu–ZrO$_2$ catalyst and those with lower Ni-content (5Ni–45Cu–ZrO$_2$ and 15Ni–35Cu–ZrO$_2$) had comparable BET surface areas of between 50 and 65 m^2 g^{-1}. The catalysts with a higher Ni-content (35Ni–15Cu–ZrO$_2$ and 45Ni–5Cu–ZrO$_2$) showed BET surface areas of 90–110 m^2 g^{-1}. N$_2$O adsorption experiments revealed more significant differences in total metal surface area between materials. Single metal catalysts, 50Ni–ZrO$_2$ and 50Cu–ZrO$_2$, have relatively low metal surfaces areas, consuming only 380 and 580 μL g^{-1} of N$_2$O, respectively. Mixed Cu/Ni materials have higher measured metal surface areas and this increases with the amount of Ni incorporated. The maximum metal surface area (3160 μL g^{-1}), was obtained

Table 2. Physical properties of materials *x*Cu-*y*Ni–ZrO₂.

Catalyst	Alloy particle size[a]/nm	BET surface area[b]/m² g⁻¹	Specific adsorption of N₂O[c]/μL g⁻¹
50Cu–ZrO₂	–	60	580
5Ni–45Cu–ZrO₂	20	50	670
15Ni–35Cu–ZrO₂	15	65	1440
35Ni–15Cu–ZrO₂	9	90	1580
45Ni–5Cu–ZrO₂	7	110	3160
50Ni–ZrO₂	–	80	380

[a]Average particle sizes of the Ni–Cu alloy species calculated using the Scherrer equation at 2θ = 42–46°.
[b]BET surface area.
[c]N₂O adsorption data of catalysts prepared with different Cu–Ni content.

for the 45Ni–5Cu–ZrO₂ material and is around six times that of the pure metal samples. The results can be related to the catalytic activity shown in Figure 1. The most active catalyst (45Ni–5Cu–ZrO₂) had the highest BET surface area and the highest specific adsorption of N₂O, whereas the least active catalyst of the series (5Ni–45Cu–ZrO₂) showed the lowest BET surface area and lowest specific adsorption of N₂O.

The above results indicate that surface area is an important parameter in the activity of catalysts for LA hydrogenation as reported previously for Cu–ZrO₂ [5]. The most active catalyst (45Ni–5Cu–ZrO₂) has both the highest BET surface area and a high specific adsorption of N₂O with small metal particle sizes, indicating high metal dispersion in this material. The high dispersion coupled with low Cu content may also lead to more regions of exposed Ni metal available to catalyse hydrogenation [26,41].

TPR analysis was carried out on all catalysts after calcination at 550 °C before reduction in 5% H₂/Ar at 400 °C and the resulting profiles are shown in Figure 5.
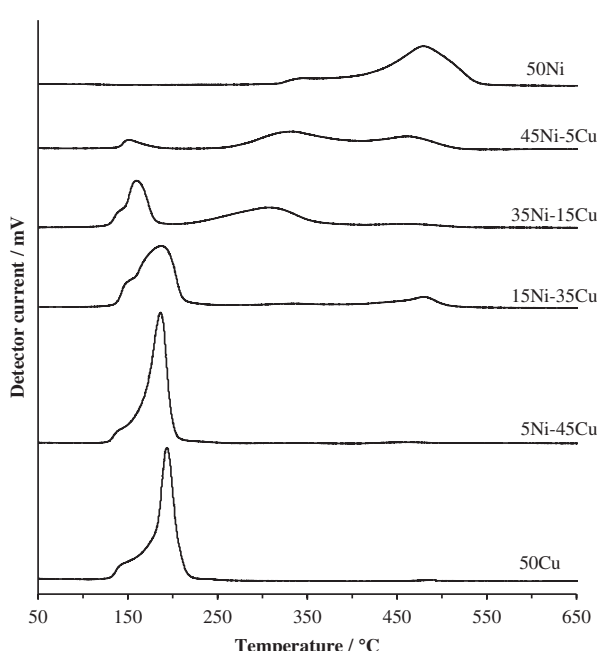

Figure 5. TPR profiles of *x*Ni–*y*Cu–ZrO₂ catalysts, compositions as indicated for each trace.

Only Cu and Ni species were reduced under the TPR conditions employed; there was no reduction signal observed for ZrO₂. From the 50Cu–ZrO₂ profile it can be seen that Cu oxide showed a reduction signal between 140 and 210 °C. 50Ni–ZrO₂ showed a reduction signal between 325 and 500 °C with a reduction temperature of approximately 450 °C. This indicates that a proportion of Ni oxide present was not fully reduced under the post-synthesis reduction conditions employed for the materials used for the catalytic data reported in Figure 1. This was confirmed by the presence of NiO peaks observed in the XRD patterns (Figure 4). The presence of NiO in the catalyst could also explain why low N₂O adsorption was observed for 50Ni–ZrO₂ (Table 3). With an increase in Ni content and a corresponding decrease in Cu content, there was a decrease in the Cu reduction signal intensity. There was no observable signal corresponding to Ni reduction in 5Ni–45Cu–ZrO₂, presumably due to the small amount of Ni present. In addition to signals corresponding to CuO reduction at 150 and 200 °C, 15Ni–35Cu–ZrO₂ showed a low intensity reduction signal corresponding to NiO at a temperature of 480 °C. The catalysts with higher Ni-content (35Ni–15Cu–ZrO₂ and 45Ni–5Cu–ZrO₂) showed a very different reduction profile compared to the lower Ni-content catalysts (5Ni–45Cu–ZrO₂ and 15Ni–35Cu–ZrO₂). Extra reduction signals between 250 and 400 °C were observed in both 35Ni–15Cu–ZrO₂ and 45Ni–5Cu–ZrO₂ which likely corresponds to the lower temperature reduction of NiO facilitated by the presence of Cu. The facile reduction of NiO due to interaction of Cu has been well documented by Arias and co-workers [26]. It is also possible that the reduction signal between 250 and 400 °C was due to the Cu–Ni alloy suggested by the XRD data (Figure 4).

XPS analysis was carried out on all catalysts and the analysis data are presented in Table 3. The binding energies of 50Cu–ZrO₂ and 50Ni–ZrO₂ were 932.9 eV and 854.9 eV respectively. The Cu(2p₃/₂) binding energy decreased as the amount of Cu in the catalyst decreased. This phenomenon was also observed in a study of Cu-doped Ni/Al₂O₃ catalysts by Naghash et al. [42] where they reported a gradual decline in binding energy of Cu with a decrease in amount of Cu doped onto the catalyst. This shift in Cu(2p₃/₂) binding energy can be attributed to the formation of less "bulk-like" Cu [43]. The Ni(2p₃/₂) binding energy increased to 855 eV when Cu was present in the catalyst, but was relatively unaffected by the amount of Cu present. The higher Ni(2p₃/₂) binding energy in the presence of Cu is indicative of a charge transfer interaction from Cu to Ni as previouly reported by Naghash et al. [42] Charge tranfer to Ni from a secondary metal has been known to facilitate the reduction of NiO at lower temperatures [44,45], as observed in our own TPR profiles of 35Ni–15Cu–ZrO₂ and 45Ni–5Cu–ZrO₂ (Figure 5). XPS therefore seems to support the idea that an alloy or solid solution was

formed on the catalyst surface when Cu and Ni are both used in the catalyst synthesis.

To consider the electronic effect of alloying Cu and Ni DFT calculations were employed to look at the band structure as a function of composition. The adsorption and dissociation of H_2 on transition metal surfaces has been related to the availability of d-electrons in the band structure of the metals through the d-band centre model [46,47]. It is possible to bring about shifts in the d-band centre through strain effects [48]. However, the close match between the atomic radii of Cu and Ni means that strain effects due to alloying are likely to be minimal and the position of the d-band centre will be largely determined by electronic effects in Cu/Ni alloys. Calculated density of states (DOS), marked with the corresponding d-band centres, for bulk Ru, Ni and Cu are presented in Figure 6. This data clearly indicates bulk Cu has the lowest d-band centre followed by Ru and then Ni. As a magnetic metal, Ni shows a shift between the up and down spin DOS so that the d-band centres are of different energies. According to the d-band centre concept a high lying d-band centre would be expected to indicate a propensity for chemisorption of H_2 to produce surface adsorbed H atoms.

Figure 6 shows that the highest d-band centre for the three metals is for Ni with the minority spin population having a d-band centre at -1.44 eV. The Ru d-band has a different shape to that of the other two metals covering a broader energy range and consequently has a generally lower amplitude. This places the d-band centre at -1.99 eV although there are clearly d-states at the Fermi level. In contrast the d-band of Cu is practically filled and so this metal has the lowest lying d-band centre at -2.75 eV consistent with its expected lower activity for H_2 adsorption. The differing d-band centre values correlate well with the different adsorption behaviours between the metals reported in the literature for H_2. For Cu (110) Campbell et al. [49] report an experimentally determined activation energy for dissociative adsorption of hydrogen of 59.83 ± 5.85 kJ mol^{-1}, whilst theoretical calculations by Yang et al. [50] determined the lowest barrier to dissociation of H_2 on various sites on Ni (111) to be 6.69 kJ mol^{-1}. As the dissociation of hydrogen on active metal particles is vital in the conversion of LA to GVL the d-band centre analysis would suggest that Ni rich catalysts should be more effective than Cu based materials.

In order to investigate the effect of alloying Cu and Ni on the d-band centre a 2 × 1 supercell of Cu was taken and doped sequentially via the thermodynamically most stable composition to form bulk Ni. A plot of the calculated d-band centre against the mole fraction Ni in bulk Cu is presented in Figure 7. Up to 0.2 mol fraction of Ni in Cu the up and down spin state DOS give an identical d-band centre but they become increasingly differentiated at higher Ni loadings. Increasing the percentage of Ni in bulk Cu also increases the d-band centre of both up and down DOS up to a mole fraction of 0.6, the corresponding experimental catalyst would be denoted 30Ni–20Cu–ZrO$_2$. After this point as the Ni proportion increases, the higher lying d-band centre (labelled as spin down in Figure 7) varies only slowly and the lower lying band d-centre actually decreases. This change with Ni content suggests that the electronic structure of the resulting alloys should be more active for LA hydrogenation since the higher lying d-band centre

Table 3. XPS analysis of xNi–yCu–ZrO$_2$ catalysts.

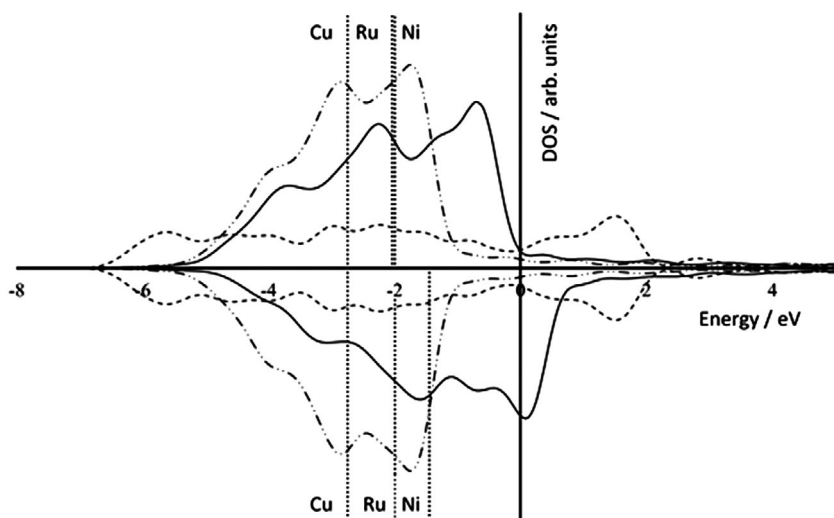| Catalyst	Binding energies/eV	
	Ni (2p$_{3/2}$)	Cu (2p$_{3/2}$)
50Cu–ZrO$_2$	–	932.9
5Ni–45Cu–ZrO$_2$	855.5	932.6
15Ni–35Cu–ZrO$_2$	855.8	932.3
35Ni–15Cu–ZrO$_2$	855.6	932.4
45Ni–5Cu–ZrO$_2$	855.3	932.1
50Ni–ZrO$_2$	854.9	–

Figure 6. DOS plots for bulk Ni (solid line), Ru (dashed line), and Cu (dot-dash line). Calculated d-band centres (in eV) are shown as dotted vertical lines labelled by metal type. Spin up states are shown as positive and spin down negative DOS values.
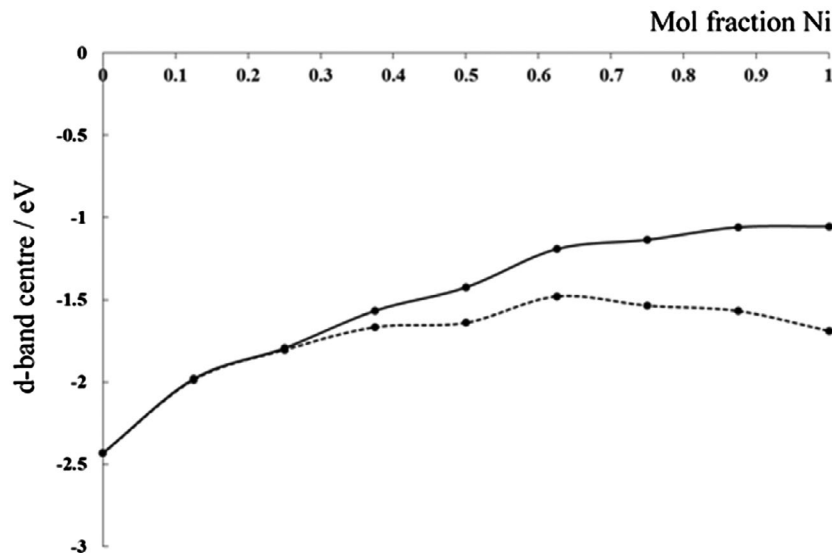
Figure 7. Calculated d-band centre as a function of Ni mole fraction in a 2 × 1 supercell of bulk Cu. Spin up (dotted line) and spin down (solid line) contributions are plotted separately, asymmetry between d-band centres becomes more pronounced as the mole fraction of Ni is increased.
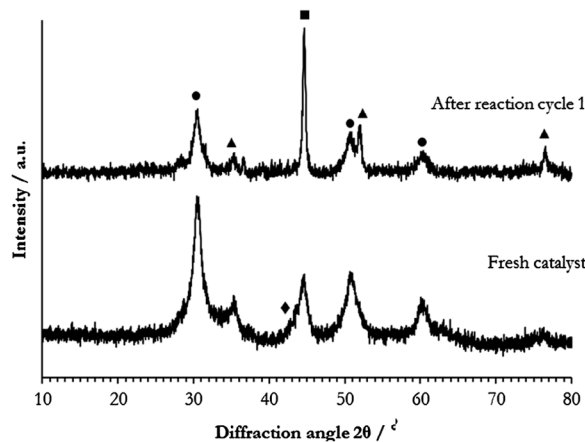

Figure 8. XRD patterns of 45Ni–5Cu–ZrO$_2$ before and after reaction. ●: ZrO$_2$; ▲: NiO; ■: Ni; ▼: Cu; ♦: Cu–Ni.

indicates that H$_2$ dissociation should become easier on the alloy metal particles with a high Ni content.

Having considered the origin of the enhanced activity of the xCu–yNi–ZrO$_2$ catalysts compared to the individual metal components catalyst lifetime and deactivation was analysed. The ability of a catalyst to maintain its activity on re-use is extremely important. Therefore, the most active Ni–Cu catalyst (45Ni–5Cu–ZrO$_2$) was tested for its activity on reuse. Reusability reactions were carried out according to the procedure outlined in the Experimental Section with all reactions performed under identical conditions. Activity data showed that there was a decline in GVL yield from 76 to 50% on reuse. Characterisation of the catalyst after the reaction was carried out to ascertain the reason for the decrease in catalytic activity.

XRD patterns were obtained for the catalysts before and after reaction cycle 1 and are shown in Figure 8. The fresh catalyst shows a broad peak in the region 42–46°

identified with metal nano-particles (see discussion with Figure 4). After reuse this peak appears sharper and is centred on 2θ = 44.5° corresponding to metallic Ni. From the Scherrer equation, the metal particle size was estimated to increase from 6 nm prior to the reaction to 17 nm after the reaction, suggesting significant particle sintering has taken place. The BET surface area was also found to decrease after reaction, from 110 m^2 g^{-1} for the fresh catalyst to 80 m^2 g^{-1} for the used. It has been established that high surface area, both of the material and metal, are important for high activity in xNi–yCu–ZrO$_2$ catalysts and the observed changes in these factors could explain the lower GVL yield obtained when the catalyst is reused.

MP-AES analysis was carried out on the post-reaction solutions in order to determine whether loss of metal was also partially responsible for the deactivation of the catalyst. The extent of metal leaching from all xNi–yCu–ZrO$_2$ catalysts is displayed in Table 4. There was minimal leaching of Cu from all catalysts observed during the reaction. However, there was a significant amount of Ni leaching observed.

To determine whether the leached Ni contributed to catalytic activity, the catalyst was filtered after regular reaction of 30 min, and the reaction resumed for a further 30 min without a solid catalyst present. 45Ni–5Cu–ZrO$_2$ was chosen because it was the most active catalyst and showed the largest amount of leached Ni. The result of this experiment is shown in Figure 9. The yield of GVL after 30 min in the presence of 45Ni–5Cu–ZrO$_2$ was around 75%. The yield of GVL remained unchanged after removal of the catalyst and further reaction for 30 min. This indicates that the reaction was entirely heterogeneous and the leached metal did not play any role in the reaction.

Table 4. Metal leaching from the xNi–yCu–ZrO$_2$ catalyst in the post-reaction solution obtained by MP-AES.

Sample	Cu leaching/ppm	Ni leaching/ppm
50Cu–ZrO$_2$	0.2	n/a
5Ni–45Cu–ZrO$_2$	0.3	25.2
15Ni–35Cu–ZrO$_2$	0.2	36.4
35Ni–15Cu–ZrO$_2$	1.5	24.9
45Ni–5Cu–ZrO$_2$	0.2	42.9
50Ni–ZrO$_2$	n/a	39.4

Figure 9. The effect of leached metal on GVL yield. ●: 45Ni–5Cu–ZrO$_2$ catalyst present (0.05g); ○: 45Ni–5Cu–ZrO$_2$ removed after 30 min. *Reaction conditions:* 200 °C, 35 bar H$_2$, 5 wt.% LA/H$_2$O.

Table 5. Metal leaching from 45Ni–5Cu–ZrO$_2$ after reaction with various substrates.

Substrate	Cu leaching/ppm	Ni leaching/ppm
Levulinic acid	0.2	42.9
GVL	0.0	9.7
Pentanoic acid	0.2	16.2
2-Pentanone	0.1	3.0

To determine if leaching is caused by interaction of the metal with reactant, reaction intermediates or the product, tests were carried out using each of LA, GVL and the model compounds 2-pentanone and pentanoic acid. Each was used for a reaction using 45Ni–5Cu–ZrO$_2$ as a catalyst under normal reaction conditions. 2-Pentanone and pentanoic acid were selected because they represent the ketone and carboxylic acid functionalities present in LA. The resulting reaction mixtures underwent MP-AES analysis to determine the metal content (Table 5). In all cases minimal Cu leaching was observed. However, there was a variation in the amount of Ni leached from the catalyst into solution. LA caused more Ni leaching than GVL indicating that the reagent is mainly responsible for Ni leaching. Comparison of the data for the model compounds pentanoic acid and 2-pentanone shows that the carboxylic acid functionality of LA is the likely cause of the observed metal leaching.

Conclusions

A series of xNi–yCu–ZrO$_2$ catalysts with $x + y = 50$ mol % but varying Ni–Cu composition were prepared by an OG method and were found to be active for LA hydrogenation, with 45Ni–5Cu–ZrO$_2$ producing a GVL yield of 76% in 30 min when the catalyst was prepared with

a 400 °C reduction step after synthesis. XRD analysis and XPS measurements showed the formation of Ni–Cu alloy particles in the mixed metal catalysts. It was generally found that Ni-rich catalysts were more active than Cu-rich catalysts. These materials showed the small particle sizes of the alloy species as measured by XRD, large BET surface areas and large number of exposed metallic sites as shown by adsorption of N$_2$O.

DFT calculations show that the d-band centre moves to higher energies as a function of Ni loading in Ni–Cu alloys, suggesting that there is also an electronic advantage to having alloy particles containing a large proportion of Ni. The high lying d-band centre is known to be a good predictor of the ability of a metal to dissociated H$_2$, which is likely to be the key step in LA hydrogenation.

TPR analysis indicated that the reduction temperature of NiO was decreased by the presence of Cu, which would suggest that a greater proportion of reduced metal is present under reaction conditions.

MP-AES analysis, also showed that a significant leaching of Ni occurred during the reaction while only minimal leaching of Cu was observed. Reusability tests were conducted for the 45Ni–5Cu–ZrO$_2$ catalyst. It was found out that the catalyst activity was reduced after one use from a GVL yield of 76 to 50%. Deactivation was attributed to particle sintering and Ni leaching promoted by the carboxylic acid group of LA.

This study provides a new direction for the design of the bimetallic catalyst based on novel, cheap and abundant metals. Catalyst deactivation with re-use is still a significant hurdle to the practical application of these catalysts. We are currently exploring the use of a flow reactor, as by shortening the LA contact time with the catalyst we expect to be able to reduce the loss of Ni metal through leaching.

ORCID

Sarwat Iqbal http://orcid.org/0000-0002-2210-4412
Satoshi Ishikawa http://orcid.org/0000-0003-4372-4108
David J. Willock http://orcid.org/0000-0002-8893-1090

References

[1] Bozell JJ, Petersen GR. Technology development for the production of biobased products from biorefinery carbohydrates – The US Department of Energy's "Top 10" revisited. Green Chem. 2010;12:539–554.

[2] Corma A, Iborra S, Velty A. Chemical routes for the transformation of biomass into chemicals. Chem Rev. 2007;107:2411–2502.

[3] Paul SF. Alternative fuel. patent WO1997043356 A1. 1997.

[4] Geilen FMA, Engendahl B, Harwardt A, et al. Selective and flexible transformation of biomass-derived platform chemicals by a multifunctional catalytic system. Angew Chem Int Ed. 2010;49:5510–5514, S5510/5511-S5510/5510.

[5] Jones DR, Iqbal S, Ishikawa S, et al. The conversion of levulinic acid into γ-valerolactone using Cu–ZrO$_2$ catalysts. Catal Sci Technol. 2016;6:6022–6030.

[6] Liguori F, Moreno-Marrodan C, Barbaro P. Environmentally friendly synthesis of γ-valerolactone by direct catalytic conversion of renewable sources. ACS Catal. 2015;5:1882–1894.

[7] Amenuvor G, Makhubela BCE, Darkwa J. Efficient solvent-free hydrogenation of levulinic acid to γ-Valerolactone by pyrazolylphosphite and pyrazolylphosphinite Ruthenium(II) complexes. ACS Sustainable Chem Eng. 2016;4:6010–6018. DOI:10.1021/acssuschemeng.6b01281

[8] Piskun AS, van de Bovenkamp HH, Rasrendra CB, et al. Kinetic modeling of levulinic acid hydrogenation to γ-valerolactone in water using a carbon supported Ru catalyst. Appl Catal A. 2016;525:158–167.

[9] Michel C, Zaffran J, Ruppert AM, et al. Role of water in metal catalyst performance for ketone hydrogenation: a joint experimental and theoretical study on levulinic acid conversion into gamma-valerolactone. Chem Commun. 2014;50:12450–12453.

[10] Yan K, Lafleur T, Wu G, et al. Highly selective production of value-added γ-valerolactone from biomass-derived levulinic acid using the robust Pd nanoparticles. Appl Catal A. 2013;468:52–58.

[11] Liu Y, Sun Z, Huang C, et al. Efficient hydrogenation of biomass oxoacids to lactones by using NHC–Iridium coordination polymers as solid molecular catalysts. Chem Asian J. 2017;12:355–360. DOI:10.1002/asia.201601537

[12] Xu S, Yu D, Ye T, et al. Catalytic transfer hydrogenation of levulinic acid to γ-valerolactone over a bifunctional tin catalyst. RSC Adv. 2017;7:1026–1031.

[13] Qiao Y, Said N, Rauser M, et al. Preparation of SBA-15 supported Pt/Pd bimetallic catalysts using supercritical fluid reactive deposition: how do solvent effects during material synthesis affect catalytic properties? Green Chem. 2017;19:977–986. DOI:10.1039/C6GC02490D

[14] Hengne AM, Rode CV. Cu–ZrO$_2$ nanocomposite catalyst for selective hydrogenation of levulinic acid and its ester to γ-valerolactone. Green Chem. 2012;14:1064–1072.

[15] Yuan J, Li S-S, Yu L, et al. Copper-based catalysts for the efficient conversion of carbohydrate biomass into γ-valerolactone in the absence of externally added hydrogen. Energy Environ Sci. 2013;6:3308–3313.

[16] Ishikawa S, Jones DR, Iqbal S, et al. Identification of the catalytically active component of Cu–Zr–O catalyst for the hydrogenation of levulinic acid to γ-valerolactone. Green Chem. 2017;19:225–236.

[17] Wang L-C, Liu Q, Chen M, et al. Structural evolution and catalytic properties of nanostructured Cu/ZrO$_2$ catalysts prepared by oxalate gel-coprecipitation technique. J Phys Chem C. 2007;111:16549–16557.

[18] Cai B, Zhou X-C, Miao Y-C, et al. Enhanced catalytic transfer hydrogenation of ethyl levulinate to γ-valerolactone over a robust Cu–Ni bimetallic catalyst. ACS Sustainable Chem Eng. 2017;5:1322–1331.

[19] Hengst K, Schubert M, Carvalho HWP, et al. Synthesis of γ-valerolactone by hydrogenation of levulinic acid over supported nickel catalysts. Appl Catal A. 2015;502:18–26.

[20] Mohan V, Venkateshwarlu V, Pramod CV, et al. Vapour phase hydrocyclisation of levulinic acid to γ-valerolactone over supported Ni catalysts. Catal Sci Technol. 2014;4:1253–1259.

[21] Mohan V, Raghavendra C, Pramod CV, et al. Ni/H-ZSM-5 as a promising catalyst for vapour phase hydrogenation of levulinic acid at atmospheric pressure. RSC Adv. 2014;4:9660–9668.

[22] Varkolu M, Velpula V, Burri DR, et al. Gas phase hydrogenation of levulinic acid to γ-valerolactone over supported Ni catalysts with formic acid as hydrogen source. New J Chem. 2016;40:3261–3267.

[23] Shimizu K-I, Kanno S, Kon K. Hydrogenation of levulinic acid to γ-valerolactone by Ni and MoO$_x$ co-loaded carbon catalysts. Green Chem. 2014;16:3899–3903.

[24] Upare PP, Lee J-M, Hwang YK, et al. Direct hydrocyclization of biomass-derived levulinic acid to 2-methyltetrahydrofuran over nanocomposite copper/silica catalysts. ChemSusChem. 2011;4:1749–1752.

[25] Upare PP, Jeong M-G, Hwang YK, et al. Nickel-promoted copper–silica nanocomposite catalysts for hydrogenation of levulinic acid to lactones using formic acid as a hydrogen feeder. Appl Catal A. 2015;491:127–135.

[26] Obregón I, Gandarias I, Miletić N, et al. One-pot 2-methyltetrahydrofuran production from levulinic acid in green solvents using Ni–Cu/Al$_2$O$_3$ catalysts. ChemSusChem. 2015;8:3483–3488.

[27] Obregón I, Gandarias I, Al-Shaal MG, et al. The role of the hydrogen source on the selective production of γ-valerolactone and 2-methyltetrahydrofuran from levulinic acid. ChemSusChem. 2016;9:2488–2495.

[28] Blöchl PE. Projector augmented-wave method. Phys Rev B Condens Matter. 1994;50:17953–17979.

[29] Kresse G, Joubert D. From ultrasoft pseudopotentials to the projector augmented-wave method. Phys Rev B Condens Matter Mater Phys. 1999;59:1758–1775.

[30] Kresse G, Hafner J. *Ab initio* molecular dynamics for liquid metals. Phys Rev B Condens Matter. 1993;47:558–561.

[31] Kresse G, Hafner J. Ab initio molecular-dynamics simulation of the liquid-metal–amorphous-semiconductor transition in germanium. Phys Rev B Condens Matter. 1994;49:14251–14269.

[32] Kresse G, Furthmüller J. Efficiency of *ab initio* total energy calculations for metals and semiconductors

using a plane-wave basis set. Comput Mater Sci. 1996;6:15–50.

[33] Kresse G, Furthmüller J. Efficient iterative schemes for *ab initio* total-energy calculations using a plane-wave basis set. Phys Rev B Condens Matter. 1996;54:11169–11186.

[34] Perdew JP, Burke K, Ernzerhof M. Generalized gradient approximation made simple. Phys Rev Lett. 1996;77:3865–3868.

[35] Perdew JP, Burke K, Ernzerhof M. Generalized gradient approximation made simple. Phys Rev Lett. 1997;78:1396.

[36] Abdelrahman OA, Heyden A, Bond JQ. Analysis of kinetics and reaction pathways in the aqueous-phase hydrogenation of levulinic acid To form γ-valerolactone over Ru/C. ACS Catal. 2014;4:1171–1181.

[37] Chalid M, Broekhuis AA, Heeres HJ. Experimental and kinetic modeling studies on the biphasic hydrogenation of levulinic acid to γ-valerolactone using a homogeneous water-soluble Ru–(TPPTS) catalyst. J Mol Catal A Chem. 2011;341:14–21.

[38] Fujita S-I, Sano Y, Bhanage BM, et al. Kinetic analysis of hydrogenation of cinnamaldehyde with a Ruthenium complex catalyst in several solvents. J Chem Eng Jpn. 2003;36:155–160.

[39] Ahmed J, Ramanujachary kV, Lofland SE, et al. Bimetallic Cu–Ni nanoparticles of varying composition (CuNi$_3$, CuNi, Cu$_3$Ni). Colloids Surf A Physicochem Eng Aspects. 2008;331:206–212.

[40] Wei Z, Yan P, Feng W, et al. Microstructural characterization of Ni nanoparticles prepared by anodic arc plasma. Mater Charact. 2006;57:176–181.

[41] Miranda BC, Chimentão RJ, Szanyi J, et al. Influence of copper on nickel-based catalysts in the conversion of glycerol. Appl Catal B Environ. 2015;166–167:166–180.

[42] Naghash AR, Xu Z, Etsell TH. Coprecipitation of nickel–copper–aluminum takovite as catalyst precursors for simultaneous production of carbon nanofibers and hydrogen. Chem Mater. 2005;17:815–821.

[43] Ashok J, Subrahmanyam M, Venugopal A. Hydrotalcite structure derived Ni–Cu–Al catalysts for the production of H$_2$ by CH$_4$ decomposition. Int J Hydrogen Energy. 2008;33:2704–2713.

[44] Zhang J, Wang H, Dalai AK. Development of stable bimetallic catalysts for carbon dioxide reforming of methane. J Catal. 2007;249:300–310.

[45] Takanabe K, Nagaoka K, Aika K-I. Improved resistance against coke deposition of titania supported cobalt and nickel bimetallic catalysts for carbon dioxide reforming of methane. Catal Lett. 2005;102:153–157.

[46] Hammer B, Norskov JK. Why gold is the noblest of all the metals. Nature. 1995;376:238–240.

[47] Nilsson A, Pettersson LGM, Hammer B, et al. The electronic structure effect in heterogeneous catalysis. Catal Lett. 2005;100:111–114.

[48] Yan K, Maark TA, Khorshidi A, et al. The influence of elastic strain on catalytic activity in the hydrogen evolution reaction. Angew Chem Int Ed. 2016;55:6175–6181.

[49] Campbell JM, Campbell CT. The dissociative adsorption of H$_2$ and D$_2$ on Cu(110): activation barriers and dynamics. Surf Sci. 1991;259:1–17.

[50] Yang H, Whitten JL. Dissociative adsorption of H$_2$ on Ni(111). J Chem Phys. 1993;98:5039–5049.